Applied Physics Letters

High power surface emitting InGaN superluminescent light-emitting diodes

Cite as: Appl. Phys. Lett. **115**, 171102 (2019); https://doi.org/10.1063/1.5118953
Submitted: 07 July 2019 . Accepted: 16 September 2019 . Published Online: 21 October 2019

R. Cahill, P. P. Maaskant, M. Akhter, and B. Corbett

Applied Physics Letters ARTICLE scitation.org/journal/apl

High power surface emitting InGaN superluminescent light-emitting diodes

Cite as: Appl. Phys. Lett. **115**, 171102 (2019); doi: 10.1063/1.5118953
Submitted: 7 July 2019 · Accepted: 16 September 2019 ·
Published Online: 21 October 2019

R. Cahill,[a] P. P. Maaskant, M. Akhter, and B. Corbett

AFFILIATIONS

Tyndall National Institute, University College Cork, Lee Maltings, Cork T12R5CP, Ireland

[a]Author to whom correspondence should be addressed: rory.cahill@tyndall.ie

ABSTRACT

A high power InGaN superluminescent light-emitting diode emitting normal to the substrate is demonstrated. The device uses a structure in which a monolithically integrated turning mirror reflects the light at both ends of the in-plane waveguide to direct amplified spontaneous emission downward through the transparent GaN substrate. Record optical peak powers of >2 W (both outputs) are reported under pulsed operation at 1% duty cycle. A broad, smooth emission spectrum with a FWHM of 6 nm centered at 416 nm is measured at peak output and ascribed to very low feedback associated with the turning mirror and antireflection coating.

Superluminescent light-emitting diodes (SLEDs) combine different aspects of LED and laser diode characteristics. Using a ridge structure, light is amplified along the length of a waveguide, and by minimizing the reflectivity of the end facets, light is allowed only a single pass of the waveguide, preventing the formation of Fabry–Pérot (FP) modes. The optical gain mechanism of amplified spontaneous emission (ASE) results in a high power, directional light source with a broad, smooth emission spectrum. These unique properties have made SLEDs subject to intensive research in the past few decades.[1–5] SLEDs were introduced for GaAs in 1973[6] using an absorbing rear facet to prevent reflections at that interface and suppress the formation of FP modes. All SLED geometries eventually result in breakdown to lasing at high currents due to parasitic feedback limiting the spectral quality of the emission. The first InGaN based blue-emitting SLED was demonstrated in 2009[1] using angled waveguides with respect to the emitting facets. A wide range of strategies have been employed in an attempt to reduce feedback to the waveguide by roughened etched facets,[4] passive absorbing regions,[2] and bent waveguide structures. The first CW operation of GaN-based SLEDs has been recently reported,[3] with record optical powers of over 450 mW,[7] spectral bandwidths >10 nm (70 meV),[8] and external quantum efficiencies of ∼20% in CW operation.[7] The unique SLED characteristics of beamed power and low temporal coherence combined with a short wavelength have seen them proposed as sources for picoprojection,[9] high resolution optical coherence tomography,[8] microdisplay applications,[10] and smart solid state lighting.[7,11] They have also been suggested as potential sources for visible light communications[12] due to the reported high modulation bandwidth.

All SLEDs reported to date have been edge-emitting devices. In this paper, we present surface-emitting SLEDs. The devices use monolithically integrated turning mirrors at both ends of a waveguide to direct the light downward through the transparent substrate. The surface-emitting geometry provides significant advantages by allowing on-wafer testing of the devices prior to packaging, which could significantly reduce production costs. The light exits the chip through the substrate and not through the active waveguide, thereby reducing the risk of catastrophic optical damage. Furthermore, we find that the antireflection coated substrate in conjunction with the turning mirrors is very effective in preventing feedback into the waveguide suppressing the formation of FP modes. In the blue-emitting devices reported here, superluminescence takes place at a current density of ∼10 kA cm^{-2}. The peak optical power of these devices was a record value of 2.2 W at room temperature under pulsed operation. This peak power was measured at a driving current of 1.5 A with 220 ns wide pulses.

The devices were fabricated on low defect density freestanding n-type GaN substrates with the epitaxial layers grown by metal organic vapor phase epitaxy. The structure consisted of a standard laser waveguide composed of a 1 μm thick *n*-type AlGaN bottom cladding layer, an active region of two InGaN quantum wells (QWs) separated by GaN barriers, an Mg-doped $Al_{0.2}Ga_{0.98}N$ electron blocking layer, a 100 nm thick *p*-type GaN waveguide layer, and a 500 nm thick *p*-type AlGaN cladding layer. The structure is completed with a heavily *p*-doped GaN cap layer. 3 μm wide ridge waveguides with a gain length of 1 mm were formed by etching to the top of the active region. Two 45° angled facets, which act as total internal reflection turning

mirrors, are etched to a depth of 1.9 μm and create the substrate-emitting devices. The transparent GaN substrate is polished to minimize scattering of the beam. A SiO_2 antireflective (AR) coating was applied to the bottom surface of the wafer to both improve the light extraction and further decrease feedback (Fig. 1).

Amplification of light in a SLED is obtained over the course of a single pass along the waveguide rather than multiple roundtrips as is the case with a laser. The output power is then dependent on the modal gain, $\Gamma g(I, \lambda)$, where Γ is the mode optical confinement factor and $g(I, \lambda)$ is the material gain. I and λ are the current and wavelength, respectively. The threshold for superluminescence is when $\Gamma g(I, \lambda) > \alpha$, where α is the intrinsic waveguide loss. The output power, P_o, from a single SLED output can then be expressed by

$$P_O(I) = \frac{A}{(\Gamma g(I,\lambda) - \alpha)} e^{(\Gamma g(I,\lambda)-\alpha)L}, \quad (1)$$

where A is related to the amount of spontaneously generated photons that are coupled into the waveguide and L is the length of the waveguide.

Figure 2 shows the light-current-voltage characteristics taken under pulsed operation along with the theoretical gain curve. 220 ns long pulses with a 1% duty cycle were used to reduce the effects of Joule heating. The optical power of the device was measured by placing a calibrated photodetector directly underneath the device to collect light from both output apertures. The peak power was calculated by dividing by the duty cycle. A superlinear increase in the output power is measured above 300 mA corresponding to a current density of 10 kA cm^{-2}. A maximum total output peak power of 2.2 W is measured after the application of the AR coating at a driving current of 1.5 A (50 kA cm^{-2}), which is the limitation of the equipment. The operating voltage of the device is between 6 V and 7 V. The external quantum efficiency (EQE) of the device at maximum power is 49%. The devices were not observed to degrade under these conditions testament to the quality of the low defect density substrate.

The gain curve of the device was extracted by fitting the light–current (L-I) characteristic with Eq. (1). The simulated gain curve shows that it is not saturated at 1.5 A, suggesting that higher optical powers could be achieved at higher currents. We can deduce from the point where superluminescence begins that the waveguide loss is approximately 25 cm^{-1}. The peak optical powers provided by this device are far higher than has been previously reported.[7] The explanation for these high powers are that most edge-emitting SLEDs use an absorbing back facet to limit feedback, while our devices emit from

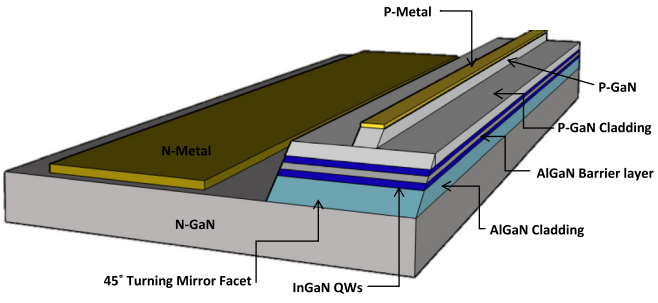

FIG. 1. Schematic of blue surface emitting LED. The sloped waveguide ends divert light downward through the transparent substrate.

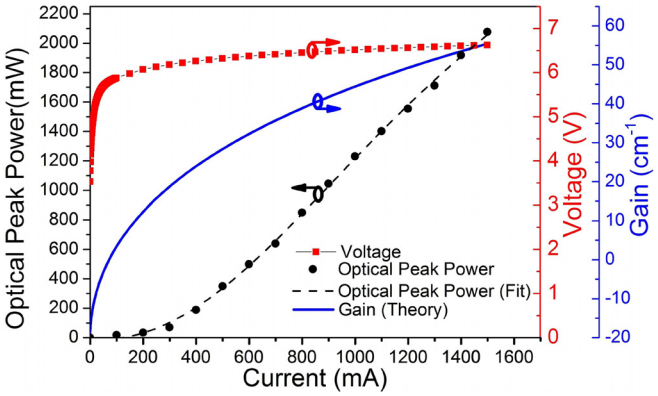

FIG. 2. Light–current-voltage characteristics of blue SLED under pulsed operation. Superluminescence is observed above 300 mA. Peak optical powers >2 W are measured. The operating voltage of the device is between 6 and 7 V. Also shown is the extracted gain as a function of current.

both ends of the waveguide, providing a significant boost to the optical power output. Figure 3 shows the intensity of the emission in the far field. This was measured by placing a scattering polymer film on glass 1 cm from the device and imaging this surface onto a CCD camera. The two intensity peaks correspond to the two turning mirrors. The asymmetry in the intensities at either side is due to a longer passive absorbing region at one end of the device than the other. The far field divergence of 7° × 15° for a single output can be extracted from this image. The divergence angles refer to the full width at half maximum (FWHM) of intensity vs angle for the individual peaks. The higher divergence in the longitudinal direction is due to tight mode confinement in the transverse waveguide.

The electroluminescence spectra of the device under pulsed operation are shown in Fig. 4, where Fig. 4(a) shows the spectra for different currents measured before the AR coating was deposited while Fig. 4(b) shows the spectra measured after the deposition. The spectra were measured on an optical spectrum analyzer with a resolution of 0.2 nm. At currents less than 300 mA, a broad spectrum with a FWHM of 26 nm is measured. At 300 mA, the ASE peak begins to emerge and the spectrum narrows to a FWHM of 6 nm (41 meV).

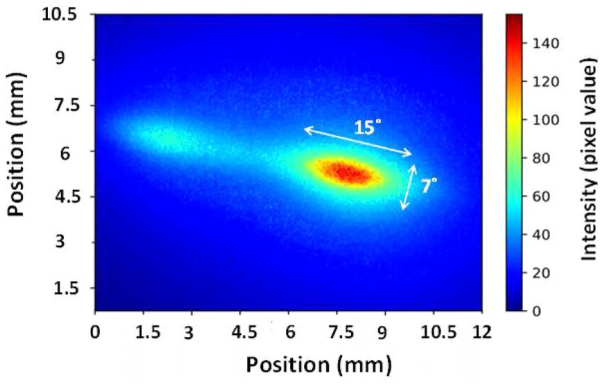

FIG. 3. Far field image of blue SLED at 500 mA. The divergence from a single output is measured to be 7° × 15°.

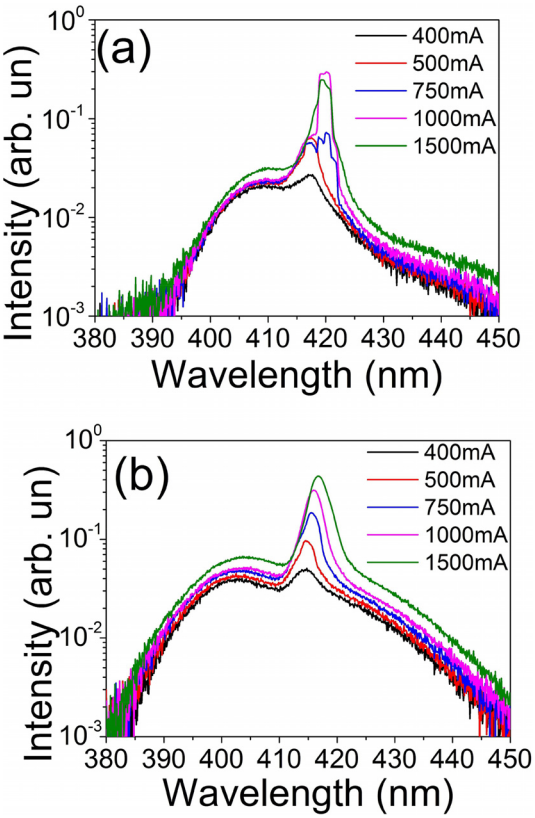

FIG. 4. Electroluminescence spectra of a blue SLED; (a) shows the spectra before antireflection coating was applied and (b) shows the spectrum after an antireflection coating had been deposited on the polished substrate.

Up to the maximum driving current of 1.5 A, the device maintains this relatively broad, smooth spectrum with a low spectral modulation depth. The device is free from parasitic lasing, which limits the spectral quality of edge emitting SLEDs. The need of the AR coating for robust SLED action is evident in Fig. 4(a), which shows that the device begins to lase at 700 mA without AR coating. The AR coating also appears to boost the amount of spontaneous emission (SE) which is extracted due to less light being lost in the chip by total internal reflection. As the device does not rely on absorbing regions to suppress feedback, lasing can be suppressed even when the optical power is very high. This suggests that the turning mirrors along with an AR coating on the substrate are extremely effective in preventing feedback in the waveguide. Figure 5 shows the spectrum of the device at maximum power on a linear scale. This shows the ASE peak as the dominant contribution to the total power. This confirms that most of the power generated in the device is directional, which should allow for better coupling into fiber based systems.

Figure 6 shows the spontaneous emission (SE) spectra, peak wavelength, and integrated intensity with increasing current under pulsed operation and collected from the top side of the chip to minimize collection of ASE. A polarizer was used to eliminate the collection of any amplified light. It is notable that the spontaneous emission intensity is not saturated even at very high current density

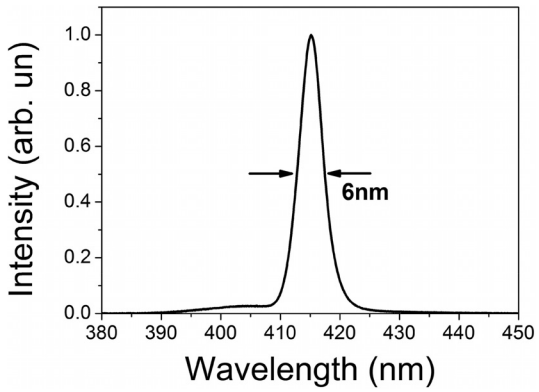

FIG. 5. Spectrum from blue SLED at 1.5 A. The peak wavelength is centered at 416 nm and the FWHM is 6 nm.

(50 kA cm^{-2} at 1.5 A), thereby indicating that there is increasing gain at this current density. The initial blueshift of the peak wavelength is attributed to the screening of the inbuilt piezoelectric field by carriers in the QWs, thereby reducing the effects of the quantum confined Stark effect. A redshift of the peak spontaneous emission from 405 nm to 410 nm at higher current densities is attributed to device heating. Using the Varshni equation, $E_g = E_g(0) - \alpha T^2/(\beta + T)$, where α and β are the material constants, E_g is the bandgap energy, and

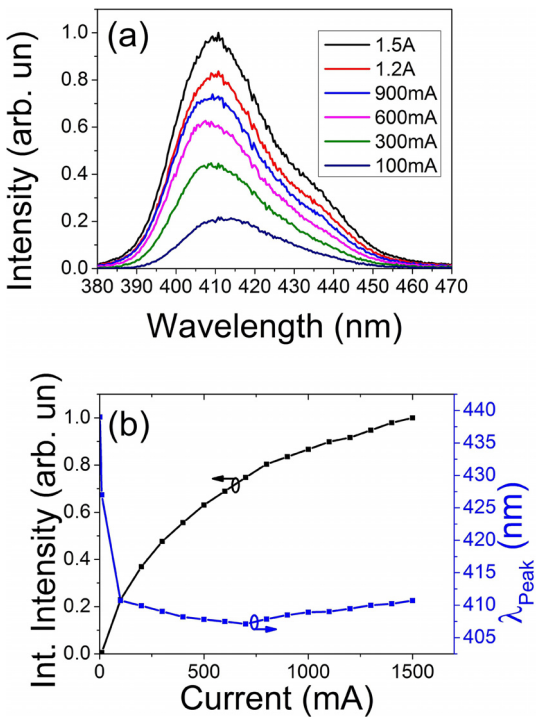

FIG. 6. (a) Evolution of the spontaneous emission spectra with current and (b) integrated spontaneous emission intensity and peak wavelength of the spontaneous emission. The spontaneous emission intensity does not saturate over the range of currents measured.

$E_g(0)$ is the bandgap energy at 0 K. By using the material constants for bulk GaN ($\alpha = 1.29 \times 10^{-3}$ eV/K and $\beta = 1280$ K)[13] a temperature increase in 110 K is calculated for the active region between threshold for superluminescence (300 mA) and the maximum current (1.5 A). The carrier temperature was extracted by measuring the derivative of the log of the intensity against energy on the high energy side of the spontaneous emission spectra.[14] An increase in the carrier temperature of ~100 K between threshold and maximum power is calculated and is in agreement with the calculated spectral shift.

Figure 7 shows the ASE spectrum where the optical peak power decreases and the peak wavelength redshifts with increasing pulse lengths as the device performance degrades due to heating. The devices reported here were measured on-wafer with no external heat management. Improved thermal management may allow for CW operation and longer pulse lengths at high currents.

We noted that the spontaneous emission spectrum of these devices continues to increase at high current density. The carrier density is expected to clamp as ASE becomes the dominant recombination mechanism and the carrier radiative lifetime is greatly reduced. As the output power is linearly dependent on the spontaneous emission rate, increasing spontaneous emission at high current density is beneficial. The distribution of photon density, $\rho(z)$, along the length, z, of a SLED waveguide can be expressed as $\rho(z) = A\{\exp[(g-\alpha)]z + \exp[(g-\alpha)(L-z)]\}/(c/n)(g-\alpha)$, where c is the speed of light, n is the group refractive index, and A is the rate of spontaneous emission coupled into the waveguide.[15] This shows a nonuniform distribution of photons across the device above threshold as shown in Fig. 8(a). By integrating the balance equation for photons and carriers,[16] $N(z) = \{J/q - cg[\rho(z)]\}\tau_{spon}/w$, where J is the current density, w is the waveguide width, q is the electron charge, d is the active region thickness, and τ_{spon} is the spontaneous emission lifetime; the distribution of carrier density N along the length of the device is shown to be nonuniform. The higher photon density near the ends of the device increases the rate of ASE in these regions. The carrier lifetime in these regions is shorter than the spontaneous emission lifetime. As photon density is lower in the center of the waveguide, fewer carriers recombine by ASE, allowing for increasing spontaneous emission in these areas. Using the relation $R_{sp} \propto N^2$, the rate of spontaneous emission along the length of the device was calculated. Integrating the calculated spontaneous emission curves shows good agreement with the increase in the intensity of the spontaneous emission that was measured. As the current increases, the carrier density and by extension spontaneous emission rate are seen to clamp first at the ends of the waveguide and then progressively toward the center until the spontaneous emission rate has saturated across the entire device. Figure 8 shows the results of these simulations and the comparison with experimental results.

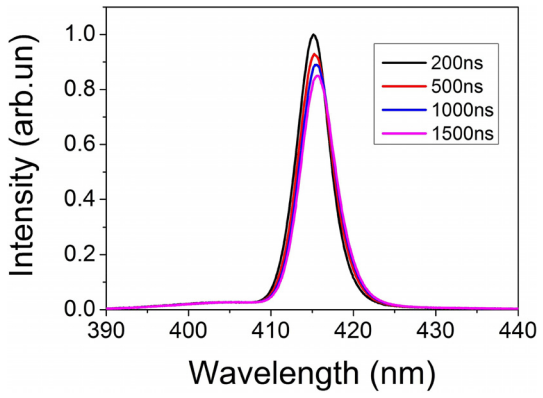

FIG. 7. ASE spectrum at different pulse lengths. The power decreases and the peak wavelength redshifts at longer pulse lengths. This indicates the effect of junction heating at longer pulse lengths.

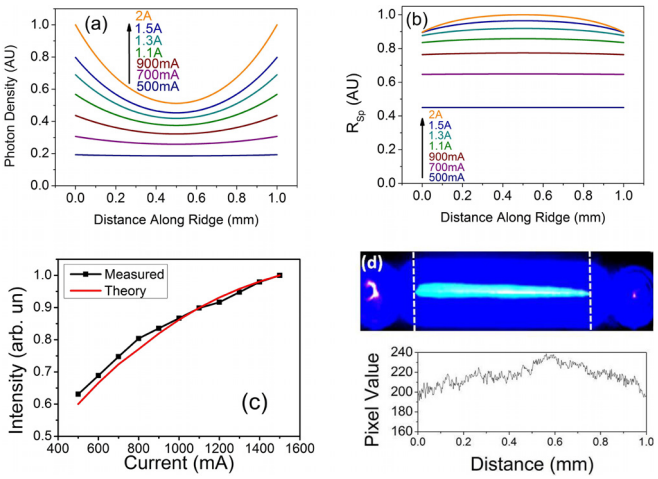

FIG. 8. (a) Calculated photon density along the waveguide as a function of current shows a nonuniform distribution of photons along the length of the waveguide; (b) spontaneous emission along waveguide; (c) comparison between the calculated and measured integrated spontaneous emission; and (d) near field image of a SLED device at 1 A with a line profile along the waveguide. This shows the highest spontaneous emission intensity in the center of the ridge. The intensity decreases closer to the ends of the waveguide in agreement with the simulations.

In summary, a surface emitting blue SLED is demonstrated with integrated turning mirrors used to direct amplified light through the substrate. A record peak optical power under the pulsed operation of 2.2 W at a 1.5 A driving current provides an external quantum efficiency of 49%. Modeling of the photon density and spontaneous emission across the ridge of the device shows that higher powers are possible at higher current densities due to increasing spontaneous emission in the center of the ridge. The combination of monolithically integrated turning mirrors and antireflection coatings is effective in reducing feedback and eliminating parasitic lasing. A broad, smooth spectrum with a FWHM of 6 nm centered at 416 nm is achieved at the maximum recorded power. The surface emitting structure provides potential for integration of further functionality onto the back side of the device increasing its potential for fiber based systems and displays.

The authors would like to acknowledge funding from Enterprise Ireland and the European Structural and Investment Funds 2014–2020 program.

REFERENCES

[1]E. Feltin, A. Castiglia, G. Cosendey, L. Sulmoni, J.-F. Carlin, N. Grandjean, M. Rossetti, J. Dorsaz, V. Laino, M. Duelk, and C. Velez, Appl. Phys. Lett. **95**(8), 081107 (2009).

[2]A. Kafar, S. Stańczyk, S. Grzanka, R. Czernecki, M. Leszczyński, T. Suski, and P. Perlin, J. Appl. Phys. **111**(8), 083106 (2012).
[3]M. Rossetti, J. Dorsaz, R. Rezzonico, M. Duelk, C. Velez, E. Feltin, A. Castiglia, G. Cosendey, J.-F. Carlin, and N. Grandjean, Appl. Phys. Express **3**(6), 061002 (2010).
[4]M. T. Hardy, K. M. Kelchner, Y.-D. Lin, P. S. Hsu, K. Fujito, H. Ohta, J. S. Speck, S. Nakamura, and S. P. DenBaars, Appl. Phys. Express **2**(12), 121004 (2009).
[5]H. Ohno, K. Orita, M. Kawaguchi, K. Yamanaka, and S. Takigawa, paper presented at the IEEE Photonic Society 24th Annual Meeting, 2011.
[6]L. Tien-Pei, C. Burrus, and B. Miller, IEEE J. Quantum Electron. **9**(8), 820 (1973).
[7]A. A. Alatawi, J. A. Holguin-Lerma, C. H. Kang, C. Shen, R. C. Subedi, A. M. Albadri, A. Y. Alyamani, T. K. Ng, and B. S. Ooi, Opt. Express **26**(20), 26355 (2018).
[8]G. R. Goldberg, A. Boldin, S. M. L. Andersson, P. Ivanov, N. Ozaki, R. J. E. Taylor, D. T. D. Childs, K. M. Groom, K. L. Kennedy, and R. A. Hogg, IEEE J. Sel. Top. Quantum Electron. **23**(6), 1 (2017).
[9]U. T. Schwarz, F. Kopp, T. Weig, C. Eichler, and U. Strauss, paper presented at the 2013 Conference on Lasers and Electro-Optics Pacific Rim (CLEOPR), 2013.
[10]M. Rossetti, A. Castiglia, M. Malinverni, C. Mounir, N. Matuschek, M. Duelk, and C. Vélez, SID Symp. Dig. Tech. Pap. **49**(1), 17 (2018).
[11]E. F. Schubert and J. K. Kim, Science **308**(5726), 1274 (2005).
[12]I. Dursun, C. Shen, M. R. Parida, J. Pan, S. P. Sarmah, D. Priante, N. Alyami, J. Liu, M. I. Saidaminov, M. S. Alias, A. L. Abdelhady, T. K. Ng, O. F. Mohammed, B. S. Ooi, and O. M. Bakr, ACS Photonics **3**(7), 1150 (2016).
[13]S. Adachi, *Properties of Semiconductor Alloys: Group-IV, III-V and II-VI Semiconductors* (John Wiley & Sons, 2009).
[14]E. F. Schubert, *Light-Emitting Diodes*, 2nd ed. (Cambridge University Press, Cambridge, 2006).
[15]J. Park and X. Li, J. Lightwave Technol. **24**(6), 2473 (2006).
[16]I. M. Joindot and C. Y. Boisrobert, IEEE J. Quantum Electron. **25**(7), 1659 (1989).